GRIFFITH UNIVERSITY

Smart ultrafiltration membrane fouling control as desalination pretreatment of shale gas fracturing wastewater: The effects of backwash water

Author

Chang, Haiqing, Li, Tong, Liu, Baicang, Chen, Chen, He, Qiping, Crittenden, John C

Published

Journal Title

Version

Version of Record (VoR)

DOI

Rights statement

Downloaded from

Griffith Research Online

Smart ultrafiltration membrane fouling control as desalination pretreatment of shale gas fracturing wastewater: The effects of backwash water

Haiqing Chang[a,b], Tong Li[c], Baicang Liu[a,b,*], Chen Chen[d], Qiping He[e], John C. Crittenden[f]

[a] College of Architecture and Environment, Sichuan University, Chengdu 610207, China
[b] Institute of New Energy and Low-Carbon Technology, Sichuan University, Chengdu 610207, China
[c] Key Laboratory for Water Quality and Conservation of the Pearl River Delta, Ministry of Education, Institute of Environmental Research at Greater Bay, Guangzhou University, Guangzhou 510006, China
[d] Litree Purifying Technology Co., Ltd, Haikou 571126, China
[e] Chuanqing Drilling Engineering Company Limited, Chinese National Petroleum Corporation, Chengdu 610081, China
[f] Brook Byers Institute for Sustainable Systems, School of Civil and Environmental Engineering, Georgia Institute of Technology, Atlanta, GA 30332, USA

ABSTRACT

Background: Increasing attention is being paid to the treatment of shale gas fracturing wastewater, including flowback and produced water (FPW). Energy-efficient pretreatment technologies suitable for desalinating and reusing FPW are of paramount importance.

Objectives: This work focused on enhanced fouling alleviation of ultrafiltration (UF) as a pretreatment for desalinating shale gas FPW in Sichuan Basin, China. The UF fouling behaviors under various backwash water sources or coagulant dosages were evaluated, and membrane surface characteristics were correlated with UF fouling. The feasibility of Fourier transform infrared (FTIR) microscope mapping technique in quantifying UF fouling was also assessed.

Methods: Various backwash water sources, including UF permeate, ultrapure water, nanofiltration (NF) permeate, reverse osmosis (RO) permeate, RO concentrate and forward osmosis (FO) draw solution, were used to clean UF membranes fouled by shale gas FPW. The UF fouling behaviors were characterized by total and non-backwashable fouling rates. Membrane surface characteristics were analyzed by scanning electron microscopy (SEM), total tension surface and FTIR spectra.

Results: Protein-like substances in terms of fluorescence intensity in the backwash water decreased with the order of UF permeate, RO concentrate, NF permeate, RO permeate and FO draw solution. Compared with UF permeate backwashing, alleviated UF fouling was observed by using demineralized backwash water including ultrapure water and RO permeate, irrespective of hollow fiber and flat-sheet membranes. NF permeate and RO concentrate after NF used as backwash water resulted in low and comparable membrane fouling with that in integrated coagulation-UF process under optimal dosage. Among the backwash water tested, FO draw solution backwashing corresponded to the lowest UF fouling rates, which were even lower than that in the presence of coagulant under optimal dosage. The superiority of these backwash water sources to UF permeate was further confirmed by SEM images and FTIR spectra. The residual foulant mass on membrane surface and the total surface tension correlated well with non-backwashable and total fouling rates, respectively.

Conclusions: FTIR microscopy was a powerful surface mapping technique to characterize UF membrane fouling caused by shale gas FPW. Backwash water sources significantly influenced the fouling of UF membranes. In the integrated UF-NF-RO or UF-FO process, RO concentrate or FO draw solution were proposed as backwash water to enhance UF fouling control and decrease waste discharge simultaneously.

1. Introduction

The shale gas revolution in the U.S. has changed the global energy structure, and a "Golden Age of Gas" was expected (IEA, 2012). As a country with the most abundant shale gas resource (technically recoverable part) in the world (US EIA, 2013), China suffers high levels of water stress (Reig et al., 2014). In Sichuan Basin, China, each horizontal well consumed 23,650–34,000 m^3 of fresh water (Chang et al., 2014;

Zou et al., 2018). Meanwhile, 19,800 m³ of fracturing wastewater including flowback and produced water (FPW) was generated for per well during the first year (Zou et al., 2018). Both volumes were larger than that required or produced in the most shale plays of U.S. (Kondash and Vengosh, 2015). Typically, high contents of suspended and dissolved inorganic ions, organics and even radioactive matters have been detected in the FPW (Barbot et al., 2013; Estrada and Bhamidimarri, 2016; He et al., 2019). The management of these large amounts of FPW causes a critical environmental concern.

Membrane desalination processes are increasingly gaining momentum in reducing total dissolved solid (TDS) in FPW for beneficial reuse (Chang et al., 2019a; Estrada and Bhamidimarri, 2016; Riley et al., 2016; Shaffer et al., 2013). Recently, nanofiltration (NF) and reverse osmosis (RO) membranes may be appropriate techniques to recycle shale gas FPW in China due to the low TDS concentrations (< 35,000 mg/L (Chen et al., 2015; Guo et al., 2018; Kong et al., 2018)). As the increase in TDS in FPW with time, more attention is paid on desalination processes that could deal with high-salinity wastewater, such as forward osmosis (FO) or membrane distillation (Chang et al., 2019a). It is a critical prerequisite for the stable operation of these desalination processes using effective pretreatment, and ultrafiltration (UF)/microfiltration (MF) shares 46% of the researches involving RO pretreatment (Jiang et al., 2017). Despite its widespread use in seawater RO system, UF membrane pretreatment is seldomly reported in shale gas FPW treatment (Chang et al., 2019a). For internal or external reuse of shale gas FPW using NF and RO membranes (Kong et al., 2018), UF membrane was assessed as a pretreatment (Chang et al., 2019b; Guo et al., 2018). The integrated UF-FO process for desalinating shale gas wastewater was also reported (Li et al., 2014), but post-treatment is usually needed to obtain the final product from the diluted draw solution.

Membrane fouling is a key factor influencing the sustainability and safety of MF/UF systems in long-duration operation. Severe and variable membrane fouling occurred when the raw shale gas FPW was filtrated (He et al., 2014; Jiang et al., 2013; Xiong et al., 2016). The fouling performance of MF/UF membrane depends on many factors, such as membrane property (Jiang et al., 2013), operating flux (Guo et al., 2018) and feed water quality (He et al., 2014), but inconsistent results have also been reported. At elevated shear stress, severe fouling could occur for ceramic and polymeric MF membranes due to floc breakage (He et al., 2014). Moreover, the fouling rate did not correlate well to turbidity, total suspended solid or total organic carbon (Xiong et al., 2016). Thus, appropriate approaches are required to eliminate fouling during ultrafiltration of shale gas FPW. On the one hand, coagulation is the widely used pretreatment to reduce the contents of organics and particulate matters (Acharya et al., 2011; Fakhru'l-Razi et al., 2009) and to eliminate UF fouling. More than 60% of UF fouling resistance could be eliminated by aluminum and iron coagulation at optimal dosage when compared to raw FPW (Chang et al., 2019b). On the other hand, backwashing with appropriate water quality took a great role in UF membrane fouling control (Chang et al., 2017). UF permeate is a commonly used backwash water, but the metrics of purer water (such as deionized water, RO permeate or NF permeate) backwashing in fouling control, have been reported (Li et al., 2009; Resosudarmo et al., 2013). In addition, backwashing using salt solutions or RO concentrate may be a potential cleaning approach for UF membrane fouling control (Chang et al., 2016b; Gao et al., 2016; Gilabert-Oriol et al., 2015), but their performance needs to be confirmed for shale gas FPW treatment.

Aiming at beneficial reuse of shale gas FPW using integrated UF-NF/RO processes, the effects of operating flux and coagulant type on UF fouling were investigated in our previous studies (Chang et al., 2019b; Guo et al., 2018). Further, this work primarily focused on alleviation of UF membrane fouling caused by shale gas FPW. In particular, we proposed the FO draw solution in UF-FO process as backwash water, and its effect on UF fouling performance was also investigated. Moreover,

the surface mapping technique using Fourier transform infrared (FTIR) microscopy has been used not only to characterize membrane fouling of model foulants (e.g., bovine serum albumin, alginate or silica colloid) at a given wavenumber (Benavente et al., 2016; Xie et al., 2017) but also to analyze complex compounds at a range of wavenumbers (Thygesen et al., 2014). Nevertheless, membrane fouling during filtration of real wastewater needs further investigation. Specifically, this study was carried out with three objectives: (a) to evaluate UF fouling behaviors under various backwash water sources or coagulant dosages, (b) to correlate membrane surface characteristics with UF fouling, and (c) to assess the feasibility of mapping technique using FTIR microcsopy in quantifying UF fouling.

2. Material and methods

2.1. Shale gas fracturing wastewater and backwash water

The shale gas fracturing wastewater (i.e., FPW) sample was collected in Sichuan Basin, China, with the detailed composition of the raw FPW summarized in previous work (Guo et al., 2018). Unless otherwise stated, the raw shale gas FPW was fed to UF membrane. With respect to backwash water, UF permeate, ultrapure water, NF permeate, RO permeate, RO concentrate (after NF) and FO draw solution (using NaCl) were employed. Ultrapure water (18.2 MΩ cm) was produced by a ULUPURE ultrapure water purification system (Chengdu, China). The NF permeate (at recovery of 70%), RO permeate (at recovery of 50%), RO concentrate (after NF at recovery of 50%) and FO draw solution (at recovery of 50%) are prepared at different points of experiment setup, as described in detail in Fig. S1 (Supporting Information). The RO concentrate was considered as backwash water not only because it could effectively clean UF membrane fouled by seawater (Gao et al., 2016; Gilabert-Oriol et al., 2015), but also due to the superiority of UF-NF-RO process in RO fouling alleviation (Alzahrani et al., 2013; Song et al., 2015). The RO flux could be greatly improved in the integrated UF-NF-RO process when compared to UF-RO process, as also confirmed in Fig. S2 (Supporting Information). These types of backwash water sources were chosen because they were obtained from desalination units with UF as a pretreatment for recycling shale gas FPW. Specifically, the integrated UF-NF, UF-RO, UF-NF-RO and UF-FO processes were typical (or potential) desalination processes in shale gas FPW treatment (Chang et al., 2019a). Moreover, UF tests using NaCl brine (by adding NaCl into RO permeate) that had the same EC to FO draw solution as backwash water were also carried out as control.

Besides, the UF fouling performance after coagulation was also investigated to compare with that under various types of backwash water. The coagulation protocol was same as described in previous literature (Chang et al., 2019b) except coagulant type. In this work, AlCl₃ (Damao Chemical Reagent Factory, Tianjin, China) with dosages of 50, 100, 200, 300, 500 and 700 mg/L was used. Note that UF membranes were backwashed using UF permeate in the integrated coagulation-UF process.

2.2. UF membranes

Polyvinylidene fluoride (PVDF) UF membranes with two configurations were employed: An outside-in hollow fiber UF membrane (Litree Co. Ltd., Haikou, China) and a flat-sheet UF membrane (Tianchuang Waterpure Equipment Co. Ltd., Hangzhou, China). Both UF membranes had the same nominal molecular weight cut-off (MWCO) of 100 kDa. The hollow fiber membrane had an outer diameter of 1.8 mm, and the fiber length was 18 cm, resulting in an effective filtration area of roughly 10 cm². The flat sheet UF membrane was round with a diameter of 23 mm, thus, the active filtration area of each flat-sheet membrane was 4.15 cm². The physicochemical properties of hollow fiber membrane and flat-sheet UF membrane are illustrated in Fig. S3 (Supporting Information). The primary parameters including

hydraulic permeability, pore diameter, water contact angle, Attenuated Total Reflectance FTIR (ATR-FTIR) and X-ray photoelectron spectroscopy (XPS) (Liu et al., 2011; Tang et al., 2007; Tang et al., 2009) were determined. The pure water permeability coefficients (normalized at 20 °C) of hollow fiber and flat-sheet membranes were 3.5 ± 0.1 and 22.4 ± 0.9 L/(m²·h·kPa), respectively. The obvious difference in hydraulic permeability was probably due to the larger average pore size of flat-sheet membrane than hollow fiber membrane (Fig. S3b), despite the same nominal MWCO. Although both membranes had similar initial contact angles (85–87°), the flat-sheet one experienced a dramatic decline in water contact angle when compared to the relative constant values of hollow fiber. As present in Fig. S3c, both virgin membranes showed the typical characteristic spectra peaks of PVDF polymer. The peaks at 1733 and 743 cm^{-1} of flat-sheet membrane represented stretching vibration C=O and C−N stretching and bending, respectively (Chen et al., 2006; Zhang et al., 2018). In addition, the presence of elements O and N on the membrane surface was further demonstrated by XPS spectra (Fig. S3d). Meanwhile, compared to an original PVDF membrane (25 mJ/m²) (Liu et al., 2011), the flat-sheet PVDF membrane displayed a larger surface tension (35 mJ/m²) (Chang et al., 2015). Therefore, the FTIR and XPS results, as well as surface tension, confirmed that the flat-sheet membrane was probably produced via a surface modification to some extent or blending with amphiphilic copolymers. Chemical composition of hollow fiber and flat-sheet PVDF membranes measured by XPS is also listed in Fig. S3e (Supporting Information). Only 5% of O and 1% of N were determined in virgin hollow fiber membrane.

Unless otherwise stated, hollow fiber membranes were used for fouling comparison with the presence of coagulation pretreatment and for membrane surface characteristics. Flat-sheet membranes were only used to investigate the effect of backwash water source on UF fouling (Section 3.2.1). Note that a virgin hollow fiber membrane module or a virgin flat-sheet membrane disc was employed for each test after soaking in pure water for least 24 h.

2.3. Experiment setup and experiment protocol

The setups for hollow fiber UF process and flat-sheet UF system are described in detail in (Chang et al., 2019b) and (Chang et al., 2016b), respectively. Periodic filtration and hydraulic backwash were conducted at room temperature (25 ± 2 °C), with each test lasting for 10 cycles. The filtration duration and backwash duration were 60 and 5 min, respectively. Here, a constant flux (50 L/(m²·h)) for filtration and backwash was employed, and the transmembrane pressure (TMP) data were recorded. Then, the fouling resistance could be obtained based on Darcy's law:

$$R = TMP/\mu J \tag{1}$$

where J is the membrane flux (m/s), and μ is the dynamic viscosity (Pa·s), which was calculated with an empirical relationship (US EPA, 2005):

$$\mu = 1.784 - (0.0575\ T) + (0.0011\ T^2) - (10^{-5}\ T^3) \tag{2}$$

where T is the water temperature (°C).

2.4. UF fouling characterization

In periodic filtration-backwash process, membrane fouling rate (FR) and the proportion of non-backwashable membrane resistance in total membrane resistance ($\triangle R_{nbw}/\triangle R_t$) were used to characterize the UF fouling performance. The schematic diagram of UF membrane resistance development is presented in Fig. 1. As shown in Fig. 1, the slope of a plot of membrane resistance (R, m^{-1}) versus the specific filtration volume (V$_s$, L/m²) (filtration volume per unit of membrane area) yielded the FR (m^{-2}).

- **Total fouling rate** (FR$_t$) is calculated using the slope of final membrane resistances (the resistance values before hydraulic backwashing were selected) versus specific filtration volume.
- **Non-backwashable fouling rate** (FR$_{nbw}$) is calculated using the slope of initial membrane resistances (the resistance values after hydraulic backwashing were selected) versus specific filtration volume.
 For a given cycle n, the $\triangle R_{nbw}/\triangle R_t$ value is determined based on proportion of non-backwashable membrane resistance in total membrane resistance:
- Change in **total membrane resistance** ($\triangle R_t$) is the difference between the final resistance ($R_{f,n}$) and initial resistance ($R_{ini,n}$) in cycle n: $\triangle R_t = R_{f,n} - R_{ini,n}$;
- Change in **non-backwashable membrane resistance** ($\triangle R_{nbw}$) is the difference between the initial resistance in cycle n + 1 ($R_{ini,n+1}$) and initial resistance in cycle n ($R_{ini,n}$): $\triangle R_{nbw} = R_{ini,n+1} - R_{ini,n}$.

Thereby, the average value obtained from the test (i.e., 10 cycles) was reported as the $\triangle R_{nbw}/\triangle R_t$.

As mentioned above, the hydraulic permeability of virgin flat-sheet UF membrane was 6.4 times higher than the virgin hollow fiber membrane, thus, the initial resistance of the flat-sheet membrane was just 15.6% of the hollow fiber membrane. Therefore, the FR values expressed in normalized forms rather than simple resistance development were employed to eliminate the difference in initial condition (i.e., resistance).

The statistical differences in fouling rates were evaluated by a two-way ANOVA (α < 0.05) by use of SPSS 20 (IBM Corp., Armonk, NY, USA). The relations between FR and membrane surface characteristics were analyzed using a Pearson correlation analysis.

2.5. Water quality analyses

Turbidity, pH and temperature were determined by a 2100Q portable turbidimeter (Hach Company, CO, USA), a PB-10 pH meter (Sartorius, Gottingen, Germany) and the mercury thermometer, respectively. Dissolved organic carbon (DOC) and UV absorbance at 254 nm (UV$_{254}$) were detected by the TOC-L organic carbon analyzer (Shimadzu, Japan) and Orion AquaMate 8000 UV–Vis spectrophotometer (Thermo Fisher Scientific Inc., MA, USA), respectively. Electrical conductivity (EC) and TDS were measured using a portable multifunctional meter from Myron L Company (CA, USA) (Ultrameter II 6PFC). A Dionex ICS-1100 Ion Chromatography from Thermo Fisher Scientific Inc. (MA, USA) was employed to detect cation concentrations using the CS12A column.

The 15-minute silt density index (SDI$_{15}$) was determined according to ASTM D4189-07 (2014) (ASTM International, 2014) using a 0.45 μm membrane filter (with diameter of 47 mm) under 207 kPa. The F-7000 fluorescence spectrophotometer (Hitachi, Japan) was employed to obtain fluorescence excitation-emission matrix (EEM) spectra of various backwash water sources. Water samples were diluted before fluorescence EEM measurement to ensure the UV absorbances for the tested ranges of each sample were < 0.05 cm^{-1} to minimize the inner filter. The excitation (Ex) and emission (Em) wavelengths were 200–400 and 200–550 nm, respectively, with a same step of 5 nm. The obtained EEM spectra were normalized to Raman units (RU) to eliminate instrument and sample biases (Murphy et al., 2010), and the maximum fluorescence intensity (F$_{max}$) was also calculated (Riley et al., 2018).

2.6. Membrane surface characterization

At the end of experiment, the UF membrane module or membrane disc was carefully taken out of the membrane tank, and the cake layer on membrane surface was scratched using a plastic plate. The accumulated mass of cake layer was determined by measuring the dry weight (using vacuum desiccator at 80 °C).
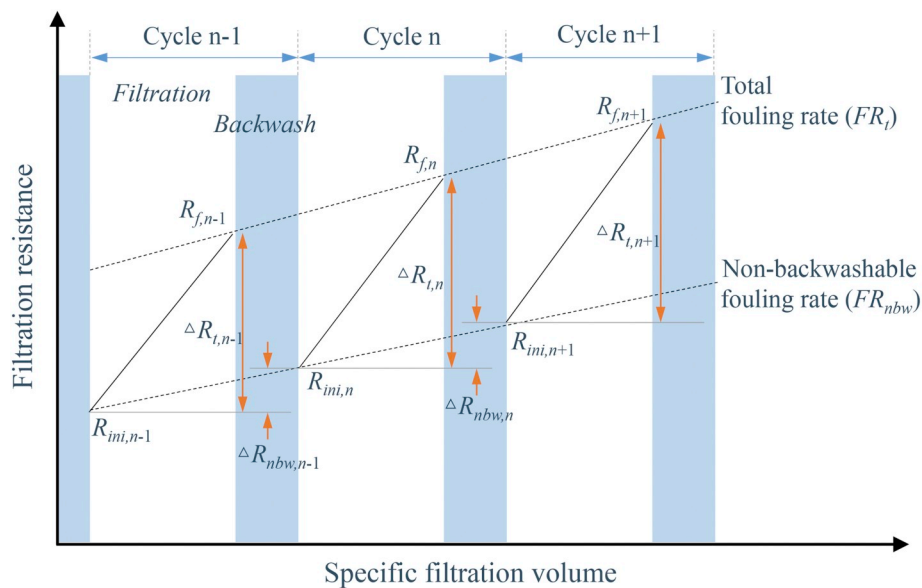
Fig. 1. The schematic diagram of UF membrane resistance development for multiple filtration/backwash cycles in constant flux operation. $R_{ini,n}$ and $R_{f,n}$ represent the initial resistance and final resistance for cycle n, respectively, while FR_t and FR_{nbw} are total fouling rate and non-backwashable fouling rate, respectively.

Table 1
Comparison of water quality characteristics of various backwash water sources (unit: mg/L[a]).

Parameters[b]	UF permeate[c]	Ultrapure water	NF permeate	RO permeate	RO concentrate	FO draw solution
DOC	12.45 ± 0.32	/	3.34 ± 0.17	1.02 ± 0.55	5.19 ± 0.49	1.30 ± 0.20
UV_{254}	0.059 ± 0.008	0.000	0.013 ± 0.001	0.003 ± 0.001	0.026 ± 0.001	0.003 ± 0.001
EC	30,980 ± 450	0.055	27,130 ± 940	463.8 ± 120.0	50,990 ± 2210	79,600 ± 3690
TDS	18,850 ± 300	/	16,270 ± 610	215.5 ± 55.7	32,300 ± 1840	58,270 ± 240
Na^+	6910 ± 40	/	5910 ± 270	86.8 ± 8.6	11,540 ± 620	21,600 ± 810
K^+	131.5 ± 2.6	/	108.9 ± 7.7	2.02 ± 1.33	208.4 ± 12.5	10.4 ± 1.0
NH_4^+	91.3 ± 1.2	/	53.7 ± 2.2	2.26 ± 0.36	107.0 ± 1.9	21.6 ± 1.3
Ca^{2+}	231.2 ± 1.8	/	82.0 ± 12.0	0.62 ± 0.22	146.9 ± 11.2	BDL[d]
Mg^{2+}	26.3 ± 0.6	/	6.3 ± 2.1	0.12 ± 0.03	12.3 ± 0.5	BDL
Ba^{2+}	133.7 ± 1.4	/	34.7 ± 8.5	0.23 ± 0.19	63.6 ± 4.5	BDL
Sr^{2+}	68.3 ± 4.4	/	20.4 ± 5.2	0.10 ± 0.06	39.0 ± 4.1	BDL

[a] All units are expressed in mg/L with the exception of UV_{254} in cm^{-1} and EC in μS/cm.
[b] Data are expressed as average value ± standard deviation.
[c] UF permeate obtained from hollow fiber membrane.
[d] BDL, below the detection limit.

The fouled UF membrane samples were dried under room condition before scanning electron microscopy (SEM) observation, contact angle measurement and FTIR scanning. Membrane surface morphology was observed by SEM (SU3500, Hitachi, Japan) at an acceleration voltage of 15 kV, after coating with gold with an etching coating system (Q150R ES, Quorum, UK). An energy dispersive spectrometer (EDS) was used to detect the elemental composition of membrane surface with a depth of few microns (Gorzalski et al., 2017) at an acceleration voltage of 15 kV, after gold-coating by a MSP-2S putter coater system (IXRF Systems Inc., USA).

The contact angle of membrane sample was measured by a DSA25S contact angle apparatus (KRÜSS GmbH, Germany), and the standard sessile drop method was employed. The surface free energy parameters ($γ^{LW}$, $γ^{AB}$ and $γ^{Tot}$) of UF membranes were calculated using three liquids (i.e., ultrapure water, glycerol and diiodomethane), with calculation procedure reported elsewhere (Chang et al., 2015).

The ATR-FTIR spectroscope (Alpha, Bruke, Germany) was used to characterize surfaces of virgin and fouled UF membranes, with a penetration depth of from < 200 nm to > 300 nm for different wavenumbers (Tang et al., 2009). The membrane samples were scanned at wavenumbers of 4000–600 cm^{-1} for 64 times at a resolution of 2 cm^{-1}.

Furthermore, membrane surfaces were analyzed using a FTIR microscopy (Spotlight 400, Perkin-Elmer Inc., Waltham, MA, USA) under reflection mode, following the protocol described in published literature (Baker et al., 2014). Membrane samples on the adjustable motorized x-y mapping stage were measured with an aperture of 25 μm, and an area of 1000 μm × 1000 μm was pre-defined. The spectra were collected with 8 scans in mid-IR spectral range of 4000–750 cm^{-1} in a 16 cm^{-1} increment. A minimum of three replicates was measured for each sample and a gold mirror was used as reference for the measurements. The maps were color coded with respect of peak height intensity (Benavente et al., 2016). The lowest intensity (0.0) was coded as blue, the highest (1.0) as red, and the intermediate colors light blue, green, yellow and orange indicated an increasing intensity from 0.0 to 1.0. Higher peaks were related to more presence of given compound(s) on membrane samples.

3. Results and discussion

3.1. Water quality characteristics of various backwash water sources

The detailed composites of various backwash water sources are listed in Table 1. The hollow fiber membrane was used because there was not a significant difference in water quality of UF permeate from

hollow fiber membrane and that from the flat-sheet membrane ($p > 0.05$) (Fig. S4, Supporting Information). In raw shale gas FPW, the UV_{254} (0.061 cm^{-1}) was much less than that in most North American plays (0.5–2.4 cm^{-1}) (Maltos et al., 2018; Sari and Chellam, 2015). Similarly, the TDS in the raw shale gas FPW (18,900 mg/L) was quite low (Barbot et al., 2013; Jiang et al., 2013; Riley et al., 2016). The primary cations are listed due to their great role in UF membrane cleaning (Chang et al., 2015; Corbatón-Báguena et al., 2014). As shown in Table 1, although low rejections were observed for monovalent cations (also for TDS and EC), a large amount of divalent cations and organics were rejected by NF membrane (Chang et al., 2019b; Kong et al., 2018; Riley et al., 2016). In contrast, the RO membrane rejected most of the cations, TDS and organics (Guo et al., 2018; Kong et al., 2018), with less residual concentrations in RO permeate. With respect to the RO concentrate, much higher concentrations of monovalent cations (e.g., Na$^+$ and K$^+$), TDS and EC were observed when compared to UF permeate, but contents of divalent cations (i.e., Ca^{2+}, Mg^{2+}, Ba^{2+}, Sr^{2+}) were greatly decreased. Similar to RO membrane, the FO membrane rejected most of organics (Table 1), with similar DOC and UV_{254} concentrations in diluted FO draw solution and in RO permeate. However, the primary cation in the diluted draw solution was Na$^+$ (21,600 mg/L), and a few monovalent ions (e.g., K$^+$ and NH$_4^+$) were

also determined, while other cations were not detectable.

Fig. 2 displays the corrected fluorescence EEM spectra for the water used for UF backwashing. Primary peaks at (I) Ex/Em = 205/315 nm and (IV) Ex/Em = 280/310 nm (Fig. 2), indicated the presence of aromatic protein and tyrosine- & protein-like substances (Chen et al., 2003), respectively. The protein-like substances have also been confirmed as the primary organic matters in FPW samples (Kong et al., 2018; Riley et al., 2016). The F_{max} at region (I) in UF permeate (4.01 RU) decreased to 0.99 and 0.20 RU for NF permeate and RO permeate, respectively, while the peak in RO concentrate reached 1.79 RU. In contrast, the lowest F_{max} value was observed for FO draw solution, with 0.12 RU at region (I). Similarly, smaller values for the F_{max} at region (IV) were observed after NF (0.53 RU) and RO treatment (0.09 RU) compared to UF permeate (2.13 RU). The F_{max} of RO concentrate at region (IV) (0.95 RU) was still much less than UF permeate, and FO draw solution showed the lowest one (0.06 RU). The normalized EEM spectra at region (IV) were much less than that obtained from the Denver-Julesburg Basin Shale (Bell et al., 2017). Therefore, the NF permeate, RO permeate, RO concentrate and even FO draw solution displayed a similar EEM distribution with UF permeate but in much lower peak intensity, consistent well with the change in organics, as seen in Fig. 2 and Table 1.
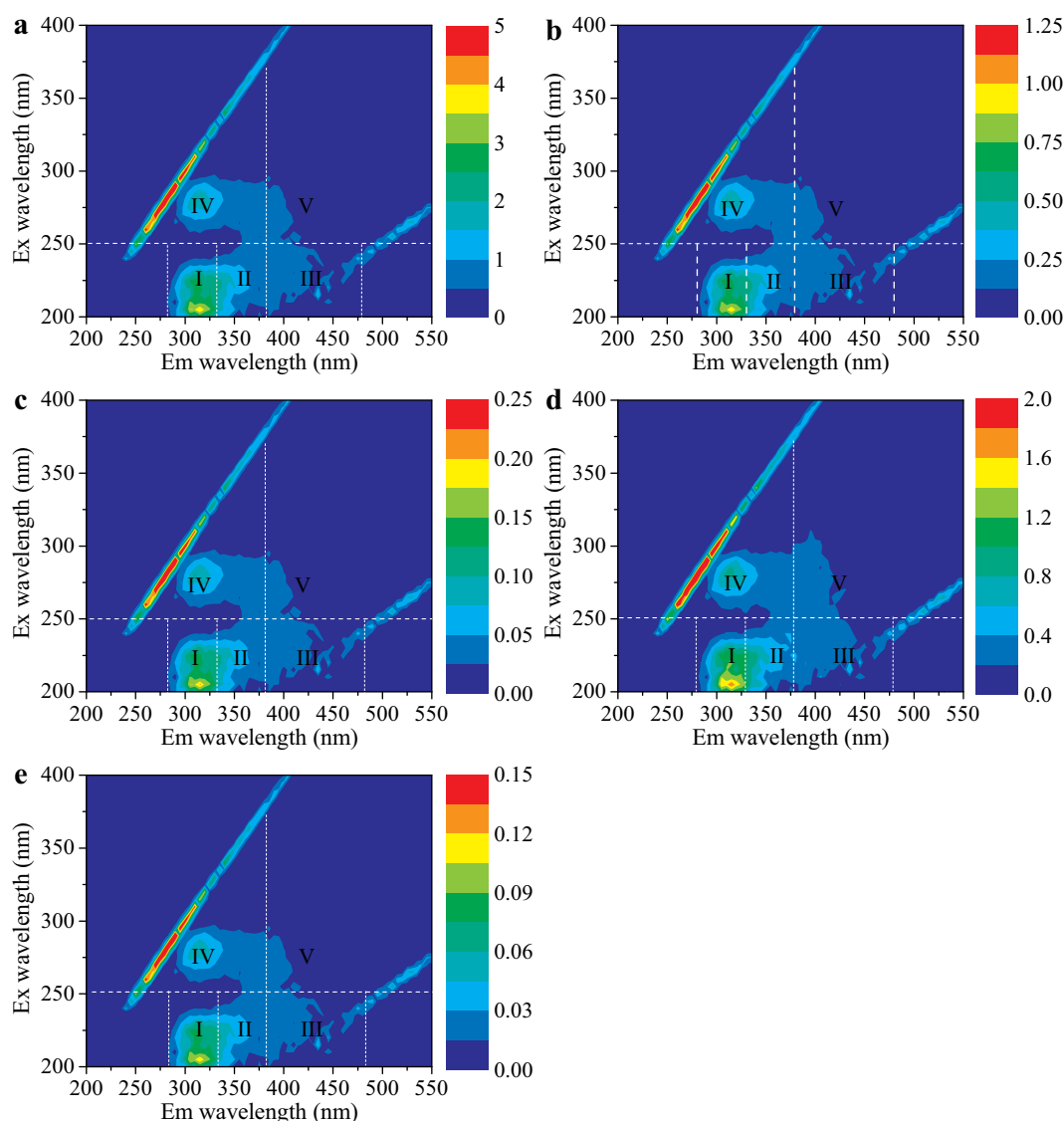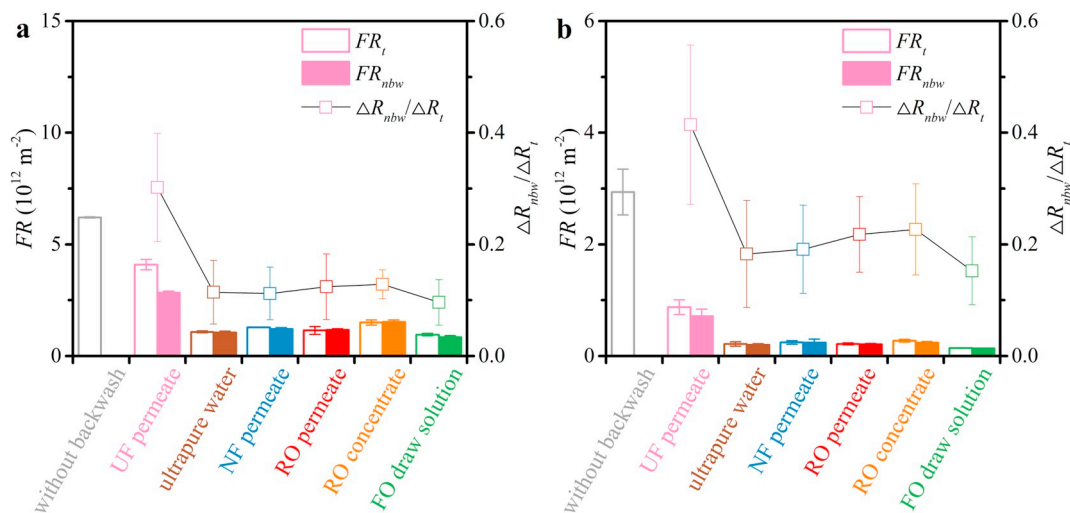

Fig. 2. Fluorescence EEM scans of backwash water used for UF membrane cleaning: (a) UF permeate, (b) NF permeate, (c) RO permeate, (d) RO concentrate and (e) FO draw solution.

Fig. 3. UF membrane fouling in terms of FR_t, FR_{nbw} and $\triangle R_{nbw}/\triangle R_t$ under various backwash water sources for both configurations: (a) hollow fiber membranes and (b) flat-sheet membranes. The FR_t and FR_{nbw} of UF membranes backwashed by NaCl brine and the difference in FR determined by ANOVA are summarized in Fig. S5 (Supporting Information).

3.2. UF membrane fouling behavior

3.2.1. Effect of backwash water source on UF membrane fouling

Fig. 3 shows FR_t, FR_{nbw} and $\triangle R_{nbw}/\triangle R_t$ of hollow fiber and flat-sheet UF membranes under various backwash water sources. When a hollow fiber membrane was employed (Fig. 3a), UF permeate backwashing led to a large FR_t ($4.09 \times 10^{12}\,\mathrm{m}^{-2}$), which was smaller than that without backwashing ($6.20 \times 10^{12}\,\mathrm{m}^{-2}$). In contrast, much smaller membrane fouling was observed when the RO permeate and ultrapure water were employed, and FR_t values decreased to 1.08×10^{12}–$1.15 \times 10^{12}\,\mathrm{m}^{-2}$. Similarly, the FR_{nbw} values of the RO permeate and ultrapure water backwashing (1.06×10^{12}–$1.17 \times 10^{12}\,\mathrm{m}^{-2}$) were also much less than the FR_{nbw} value ($2.84 \times 10^{12}\,\mathrm{m}^{-2}$) of UF permeate backwashing. The superior backwash performance of the RO permeate or ultrapure water to the UF permeate for the seawater treatment has been reported elsewhere (Resosudarmo et al., 2013). Meanwhile, the NF permeate backwashing also displayed an excellent backwash behavior, resulting in 1.29×10^{12} and $1.21 \times 10^{12}\,\mathrm{m}^{-2}$ for FR_t and FR_{nbw}, respectively. A two-way ANOVA showed that there was no significant difference in UF fouling rate including FR_t and FR_{nbw} for ultrapure water, RO permeate and NF permeate ($p \geq 0.05$), as presented in Fig. S5a (Supporting Information). The monovalent cations in the NF permeate (Table 1) did not deteriorate the UF membrane fouling performance, similar to salt backwashing of organic-fouled UF membranes (Chang et al., 2016b). The great decrease in the foulant-foulant and foulant-membrane surface interaction during the filtration of protein-like solutions (Corbatón-Báguena et al., 2014) probably led to an effective cleaning behavior of the NF permeate. Moreover, the RO concentrate backwashing resulted in small FR_t ($1.50 \times 10^{12}\,\mathrm{m}^{-2}$) and FR_{nbw} ($1.53 \times 10^{12}\,\mathrm{m}^{-2}$), though both values were slightly larger than ultrapure water backwashing, NF permeate backwashing or RO permeate backwashing ($p < 0.05$) (Fig. S5a, Supporting Information). In a seawater desalination system using UF-RO (Gao et al., 2016; Gilabert-Oriol et al., 2015), high cleaning efficiencies of UF membranes were obtained for the RO concentrate backwashing using appropriate operating approaches. For the backwash water tested, the FO draw solution backwashing displayed the lowest fouling rates, for FR_t ($0.96 \times 10^{12}\,\mathrm{m}^{-2}$) and FR_{nbw} ($0.84 \times 10^{12}\,\mathrm{m}^{-2}$). These values were statistically equal to that using NaCl brine as backwash water ($p = 0.96$ and $0.62 > 0.05$) (Fig. S5a, Supporting Information). Considering the almost same water quality of FO draw solution and NaCl brine, Na^+ in FO draw solution took a great role in UF fouling alleviation. This was attributed to the high backwash effectiveness of monovalent salt (i.e., Na^+) backwashing, and

the mechanisms including cake layer swelling and ion exchange may be involved (Section 3.5), similar to salt backwashing of UF membranes fouled by organics or real wastewater (Chang et al., 2016b). As also presented in Fig. 3a, the enhanced cleaning efficiency of ultrapure water, NF permeate, RO permeate, RO concentrate and FO draw solution was confirmed by the much lower $\triangle R_{nbw}/\triangle R_t$ values compared to that using UF permeate backwashing.

Considering the significant difference in hydraulic permeability of virgin flat-sheet membrane and hollow fiber membrane, the FR_t and FR_{nbw} values were expressed in normalized forms to eliminate the effect of membrane properties and to better characterize membrane fouling. As shown in Fig. 3b, the total fouling rate of flat-sheet UF membrane without backwashing reached $2.94 \times 10^{12}\,\mathrm{m}^{-2}$, while the UF permeate backwashing greatly decreased the FR_t ($0.87 \times 10^{12}\,\mathrm{m}^{-2}$). Compared to UF permeate backwashing, total fouling rates were much lower for the backwash water using ultrapure water, NF permeate and RO permeate ($p < 0.05$), and these backwash water sources resulted in statistically identical FR_t values (i.e., 0.21×10^{12}–$0.27 \times 10^{12}\,\mathrm{m}^{-2}$) ($p = 0.50 > 0.05$). The FO draw solution backwashing further decreased the FR_t value ($0.14 \times 10^{12}\,\mathrm{m}^{-2}$), equal to that obtained from NaCl brine backwashing ($p = 0.59 > 0.05$). As expected, much lower FR_{nbw} values were obtained when backwash water was switched from UF permeate to other backwash water sources, especially the FO draw solution (Fig. 3b). Similarly, there was not a significant difference in FR_{nbw} values of flat-sheet membranes cleaned by ultrapure water, NF permeate and RO permeate, and FR_{nbw} value for FO draw solution backwashing was statistically equal to that for NaCl brine backwashing (Fig. S5b, Supporting Information). Different to those obtained from hollow fiber membranes, the FR_t or FR_{nbw} values of flat-sheet membranes using RO concentrate backwashing were statistically identical to those using ultrapure water, NF permeate or RO permeate as backwash water, as seen in Fig. 3b and Fig. S5b. Besides, the low backwash efficiency of UF permeate was confirmed by the high $\triangle R_{nbw}/\triangle R_t$ (41.4%), while the low $\triangle R_{nbw}/\triangle R_t$ values of ultrapure water, NF permeate, RO permeate, RO concentrate and FO draw solution backwashing demonstrated their superior backwash performance. Comparing Fig. 3a and b, the fouling rates (total or non-backwashable part) of a flat-sheet membrane were lower than those of a hollow fiber membrane, but the flat-sheet membrane displayed a higher proportion of non-backwashable resistance in total resistance ($\triangle R_{nbw}/\triangle R_t$). On the whole, not only ultrapure water, NF permeate and RO permeate, but also RO concentrate and FO draw solution were more appropriate backwash water sources than UF permeate in UF fouling control.
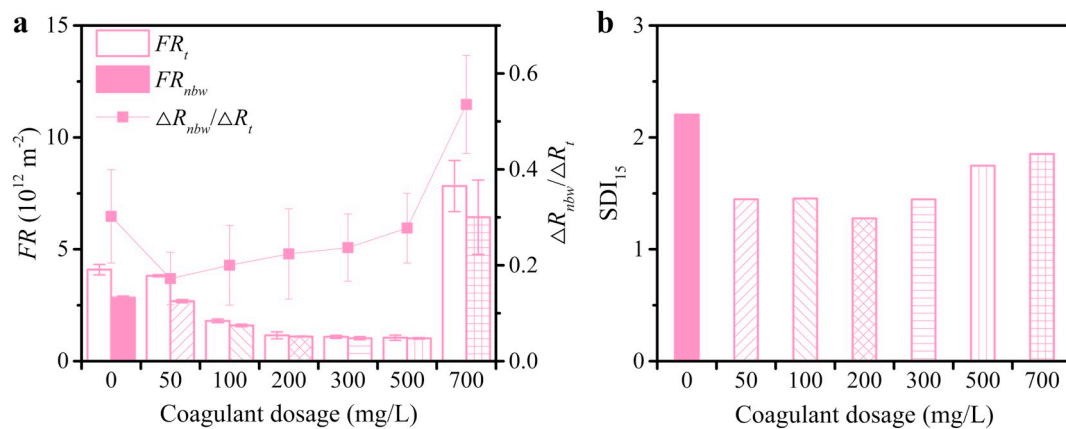
Fig. 4. UF performance for coagulated water under different coagulant dosages (AlCl₃): (a) UF membrane fouling in terms of FR_t, FR_{nbw} and $\triangle R_{nbw}/\triangle R_t$, and (b) fouling potential of UF permeate for subsequent desalination in term of SDI₁₅.
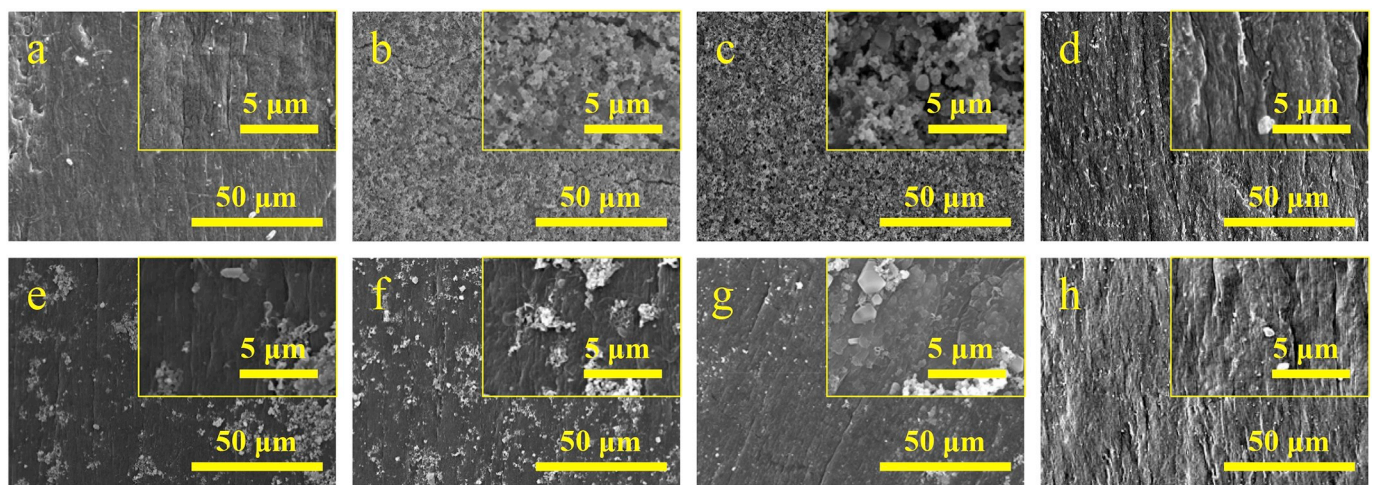

Fig. 5. SEM images of (a) virgin membrane, and UF membranes cleaned by various backwash water sources: (b) without backwashing, (c) UF permeate, (d) ultrapure water, (e) NF permeate, (f) RO permeate, (g) RO concentrate and (h) FO draw solution.

3.2.2. Comparison with coagulation-UF

Fig. 4 illustrates the impact of coagulant dosage on fouling potential and SDI₁₅ in UF permeates in the coagulation-UF process. As presented in Fig. 4a, the FR_t values decreased with the increase in AlCl₃ dosage (0–200 mg/L), and the FR_t values (1.16×10^{12}–$1.05 \times 10^{12}\,\text{m}^{-2}$) of the coagulated water for 200–500 mg/L AlCl₃ were statistically equal ($p = 0.58 > 0.05$). However, a 700 mg/L AlCl₃ dosage resulted in the largest FR_t ($7.83 \times 10^{12}\,\text{m}^{-2}$), which was also much higher than the raw water. Similar results were observed for non-backwashable fouling rate (FR_{nbw}) during ultrafiltration of coagulated water (Fig. 4a). The UF fouling performance was consistent with the water quality under different aluminum dosages, and the most severe membrane fouling at 700 mg/L was attributed to deterioration of the coagulation performance (Fig. S6, Supporting Information). In the presence of coagulant, the increase in dosage (50–700 mg/L) led to an increase in $\triangle R_{nbw}/\triangle R_t$ values, ranging from 17.2% to 53.6%, as presented in Fig. 4a. Thereby, the presence of low-dosage coagulant (< 500 mg/L) slightly resulted in enhanced backwash efficiency compared to the raw shale gas FPW.

On the whole, the AlCl₃ dosage of 200 mg/L (1.5 mmol/L Al³⁺) was appropriate for improving water quality and eliminating UF fouling (Figs. 4a and S6a). Under this dosage, the FR_t and FR_{nbw} of UF membrane were $1.16 \times 10^{12}\,\text{m}^{-2}$ and $1.10 \times 10^{12}\,\text{m}^{-2}$, 72% and 61% lower than raw water, respectively. The decrease in total and non-backwashable fouling rates were larger than those (64% and 54%) using Al₂(SO₄)₃ 18H₂O at optimal dosage (1.8 mmol/L Al³⁺) (Chang et al., 2019b). As presented in Figs. 3 and 4, the UF membrane using ultrapure water or RO

permeate backwashing had comparable fouling rate ($\sim$1.1 $\times 10^{12}\,\text{m}^{-2}$) for coagulation under optimal dosage (200 mg/L). In comparison, NF permeate or RO concentrate backwashing resulted in a slightly higher but acceptable FR_t (1.29×10^{12}–$1.50 \times 10^{12}\,\text{m}^{-2}$) or FR_{nbw} (1.21×10^{12}–$1.53 \times 10^{12}\,\text{m}^{-2}$). Furthermore, the values of FR_t ($0.96 \times 10^{12}\,\text{m}^{-2}$) and FR_{nbw} ($0.84 \times 10^{12}\,\text{m}^{-2}$) for FO draw solution backwashing were even less than those using coagulation under optimal dosage. Thus, a large amount of chemical agents (e.g., coagulant) may be saved by adjusting backwash water quality.

In addition, the SDI₁₅ values of UF permeates under different coagulant dosages were no more than 2.2, in particular for AlCl₃ dosages of 50–300 mg/L (SDI₁₅ < 1.5) (Fig. 4b). The average turbidity was < 0.10 NTU for UF permeate, and they were not significantly affected by coagulant dosage (Fig. S7, Supporting Information). These results confirmed that the pretreatment using coagulation–UF process could provide "good water quality" (SDI₁₅ < 2, turbidity < 0.1 NTU) (Voutchkov, 2010) for subsequent desalination of shale gas FPW by NF, RO or FO unit.

3.3. Correlating membrane surface characteristics with UF fouling

3.3.1. SEM-EDS observation

Fig. 5 illustrates the surface SEM observations (with magnifications of 1000 and 10,000) of the virgin hollow fiber UF membrane and fouled membranes cleaned by various backwash water sources. Compared to the smooth surface of virgin PVDF membrane (Fig. 5a), the UF

membrane without backwashing was covered with compact foulants (Fig. 5b). Similarly, a dense fouling layer was also observed on the UF membrane when periodic UF permeate backwashing was conducted, showing an inferior cleaning efficiency of UF permeate backwashing. In contrast, ultrapure water backwashing almost completely recover the virgin membrane surface (Fig. 5d), with a very small part of residual foulants deposited on the membrane surface. For UF membrane cleaned with NF permeate or RO permeate (Figs. 5e-f), only a small part of membrane surface covered with foulants after periodic backwashing, resulting in a much looser cake layer than UF permeate backwashing. Most of the foulants were also removed when RO concentrate back-washing was used (Fig. 5g), with residual foulants much less than that for UF permeate backwashing. Similar to the membrane backwashed using ultrapure water, the membrane cleaned by FO draw solution also resulted in a quite clean surface (Fig. 5h).

EDS is an appropriate technology for quantifying major elements in thick foulant layers (Gorzalski et al., 2017). The elemental compositions on the surfaces of the virgin and fouled membranes obtained from the EDS spectra are summarized in Fig. 6. As presented in Fig. 6, the major elements C and F (Suhartono and Tizaoui, 2015; Wan and Bowen, 2017) were determined, while a small amount of element O was also detected (Fig. 6), as also confirmed by XPS analysis (Fig. S3d, Supporting Information). For the fouled UF membrane without backwashing, the surface contained elements C, O, Na, Cl, Si, Ca, Fe, Sr and Ba, but element F was not detected, demonstrating the severe fouling of UF membrane. When periodic UF permeate backwashing was conducted, the membrane surface contained all the elements found in the membrane without backwashing, and a low percentage ($4.56 \pm 4.26\%$) of element F was also detected. Compared to the virgin membrane, the significant decrease for major elements C and F on membrane surfaces of these fouled membranes was confirmed using ANOVA (Table 2). Although the element C on the surface of UF membrane cleaned by NF permeate, RO permeate or RO concentrate was also statistically equal to that of virgin membrane ($p > 0.05$), a declined F content was observed for these backwash water sources ($p < 0.05$). As presented in Fig. 6 and Table 2, both the elements C and F in the membrane cleaned with ultrapure water or FO draw solution were statistically identical to those in the virgin membrane ($p > 0.05$), demonstrating the excellent backwash performance of both water sources.

3.3.2. Membrane cake layer characteristics and surface tension

Fig. 7 presents the residual deposits and surface tension of the hollow fiber UF membranes cleaned by different backwash water

Table 2
Comparison of difference in elemental composition between virgin membrane and fouled membranes under different types of backwash water using ANOVA ($\alpha = 0.05$).

Element	C	F
Virgin membrane vs. without backwash	1.54×10^{-4}	3.69×10^{-7}
Virgin membrane vs. UF permeate	1.21×10^{-3}	4.44×10^{-5}
Virgin membrane vs. ultrapure water	0.68	0.44
Virgin membrane vs. NF permeate	0.13	1.30×10^{-3}
Virgin membrane vs. RO permeate	0.56	0.02
Virgin membrane vs. RO concentrate	0.08	0.02
Virgin membrane vs. FO draw solution	0.42	0.56

sources and their relations with membrane fouling. At the end of the tests, the accumulated residual foulants in cake layer were measured, with the weight of dried cake layer per unit area of membrane surface elaborated in Fig. 7a. We found that the residual foulants on membrane surface varied with backwash water sources, and the highest value was obtained for the one without backwashing (1.24 mg/cm^2). Similarly, a high value (1.06 mg/cm^2) was observed for the residual foulant on the UF membrane backwashed by UF permeate, showing that the cake layer was thick and compact (Fig. 5c). In contrast, the mass of residual foulants greatly decreased when the backwash water was switched to ultrapure water, NF permeate, RO permeate and even RO concentrate (Fig. 7a), demonstrating the loose feature of the cake layer via SEM observation (Figs. 5d-g). In addition, the smallest residual foulant (0.37 mg/cm^2) was observed for the membrane after FO draw solution backwashing. Together with micro-observation (i.e., SEM images in Fig. 5), these values directly exhibited the difference in residual foulant on membrane surface. Further, a strong linear correlation between the residual foulants and FR_{nbw} or $\triangle R_{nbw}/\triangle R_t$ was observed (Fig. 7b), demonstrating that the non-backwashable fouling directly resulted from the residual deposits after backwashing.

As shown in Fig. 7c, the largest total surface tension (γ^{Tot}) was observed for the UF membrane without backwashing (40.0 mJ/m^2), followed by the membrane backwashed with UF permeate (38.3 mJ/m^2). Both values indicated that the transfer of surface characteristic from UF membrane to foulant (Suhartono and Tizaoui, 2015) which deposited on UF membrane surfaces to a great extent (Figs. 5b-c). In contrast, lower and comparable γ^{Tot} ($32.4\text{–}33.0 \text{ mJ/m}^2$) were found for UF membranes backwashed with ultrapure water, NF permeate, RO permeate and RO concentrate. Moreover, the membrane cleaned by FO draw solution displayed the lowest γ^{Tot} (28.6 mJ/m^2). This was
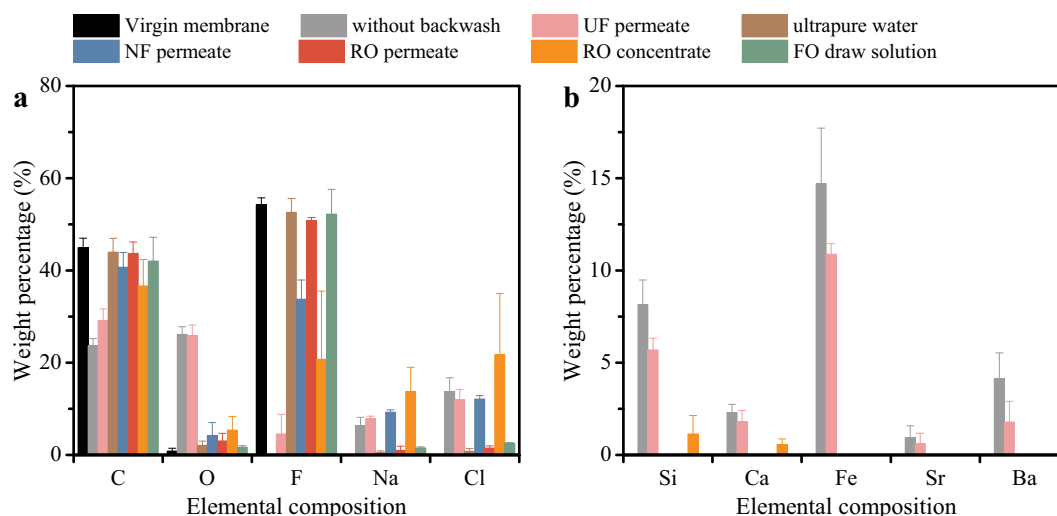
Fig. 6. Elemental contents on the surfaces of the fouled membranes under different types of backwash water identified by an EDS (error bar indicates standard deviation from average value; $n \geq 3$).
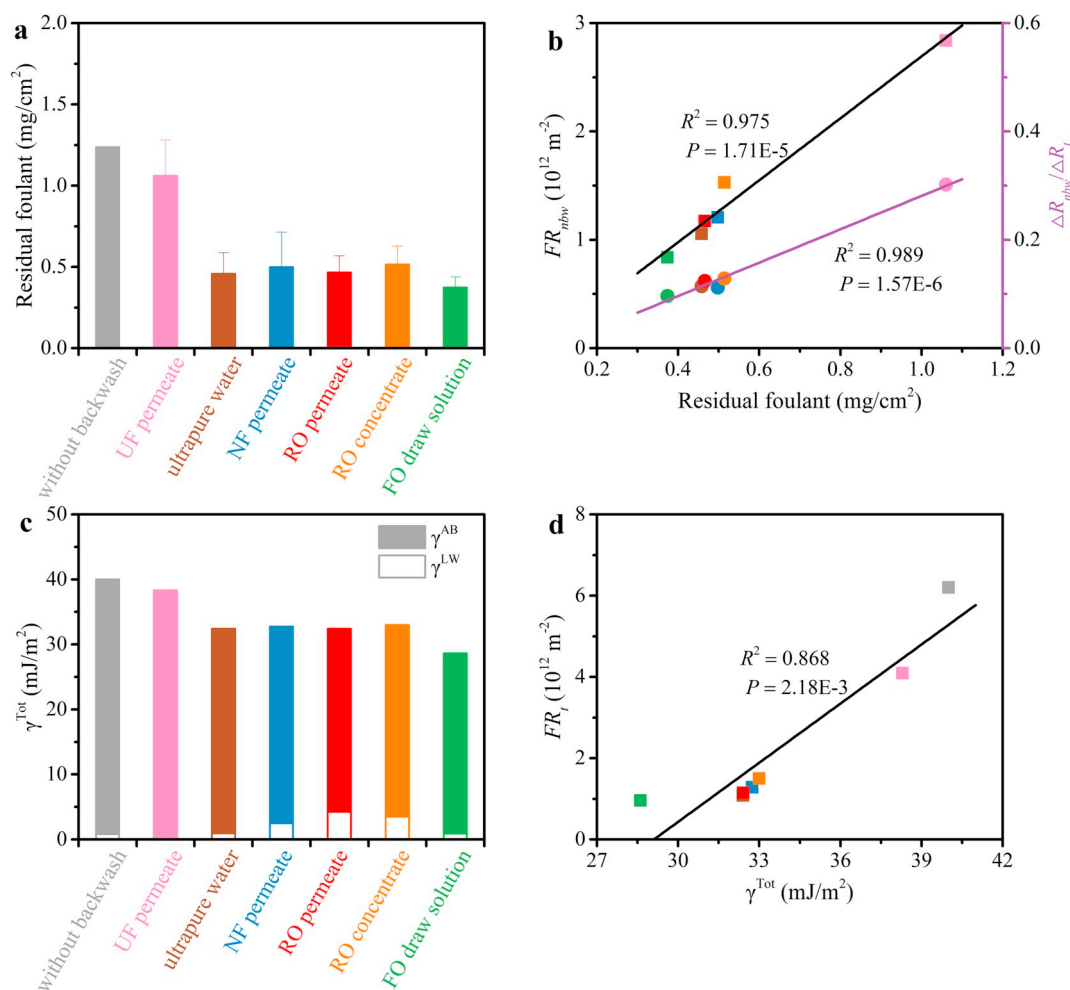
Fig. 7. UF membrane surface characteristics under various backwash water sources: (a) residual foulant in term of cake layer mass per unit area of UF membrane, (b) plot of FR_{nbw} and $\triangle R_{nbw}/\triangle R_t$ versus residual foulant, (c) surface tension (γ^{Tot}) of UF membranes, and (d) plot of FR_t versus γ^{Tot}.

probably because these membranes still remained the surface characteristics of virgin membrane (Fig. 5). Further, the values of the surface tensions of UF membranes correlated well with FR_t (Fig. 7d), indicating that the fouling propensities of UF membranes cleaned by different backwash water sources (Fig. 3) could be explained by the total surface tensions. Similar results have also been reported for surface tension and UF membrane fouling during filtration of organics (Chang et al., 2016a; Subhi et al., 2012).

3.4. ATR-FTIR spectra and FTIR microscope mapping analysis

Fig. 8 presents the FTIR spectra of fouled hollow fiber UF membrane surfaces when various backwash water sources were tested. As shown in Fig. 8, the virgin membrane showed the typical characteristic spectra peaks of PVDF. The peaks at 1178, 1070, 975, 875, 795, 763 and 615 cm^{-1} represented CF$_2$ stretching vibration, C−C symmetric stretching, CH$_2$ rocking, skeletal vibration of C−C bonds, CH$_2$ rocking, CF$_2$ bending & skeletal bending and CF$_2$ bending & skeletal bending, respectively (Suhartono and Tizaoui, 2015; Sun et al., 2018; Wan and Bowen, 2017; Zhang et al., 2013). These characteristic bands corresponded to α-phase of PVDF (Rabuni et al., 2013; Wan and Bowen, 2017). Whereas, the characteristic bands which were detected at 1402 (CH$_2$ stretching (Zhang et al., 2013)), 1275 (CF$_2$ stretching (Suhartono and Tizaoui, 2015)) and 840 cm^{-1} (skeletal C−C stretching, CH$_2$ rocking and CF$_2$ stretching (Roy et al., 2017)) were indexed to β-phase (Rabuni et al., 2013). For the raw shale gas FPW, the primary peaks

included 3407 (O−H stretching), 2919 (asymmetric CH$_2$ stretching), 2850 (symmetric CH$_2$ stretching), 1650 (amide I band) and 1540 cm^{-1} (amide II band), which were also reported in FPW samples from other raw shale gas plays (Bell et al., 2017; Du et al., 2018; Sari and Chellam, 2015). These peaks represented proteins, aliphatic hydrocarbon and humic substances (Bell et al., 2017; Du et al., 2018; Zularisam et al., 2006), these substances in raw water and thus in UF permeate as confirmed by EEM in Fig. 2. The peaks at 1440, 1402, 1178, 1092, 1021, 795, 634 and 615 cm^{-1} in the raw FPW were different to those reported in FPW from Texas (Sari and Chellam, 2015).

Compared to the virgin membrane, an obvious spectrum peak at 975 cm^{-1} was discovered for the membrane without backwashing and that backwashed by UF permeate. This phenomenon indicated that there were a large amount of matters containing CH$_2$ twisting or Si−O−C stretching, because the 975 cm^{-1} peak also represented Si−O−C stretching (Yang et al., 2017) and the element Si was also confirmed by EDS (Fig. 6). However, both membranes also displayed some typical characteristics of the raw shale gas FPW, including peaks of 3200–3550, 2919, 2850, 1650 and 1540 cm^{-1}. On the contrast, the membrane backwashed with ultrapure water maintained most of the IR spectra of the virgin membrane, although some new peaks that belonged to FPW appeared (i.e., 3200–3550, 2919, 2850, 1650 and 1540 cm^{-1}). When backwash water was switched to NF permeate or RO concentrate, the specific spectra peaks of virgin PVDF membrane decreased obviously, but three new peaks (2919, 2850 and 1540 cm^{-1}) were primarily discovered. With respect to the membrane backwashed
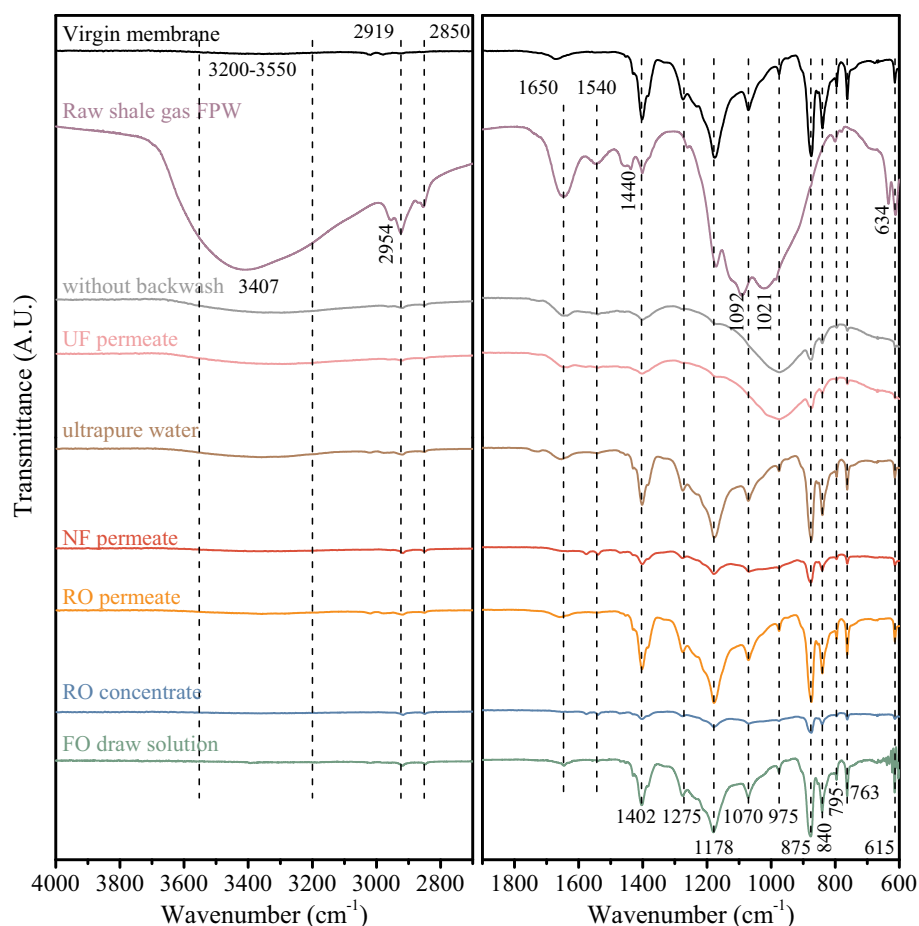
Fig. 8. ATR-FTIR of virgin membrane, raw shale gas FPW and fouled UF membranes under various backwash water sources: without backwashing, UF permeate, ultrapure water, NF permeate, RO permeate, RO concentrate and FO draw solution. (Full spectra are shown in Fig. S8, Supporting Information).

by RO permeate or FO draw solution, similar FTIR spectra peaks to that using ultrapure water backwashing were observed but with a weak band at 3200–3550 cm^{-1}.

The FTIR microscope maps of UF membranes are illustrated in Fig. 9, with related visible images in Fig. S9 (Supporting Information).

Compared to the blue color of the virgin membrane (Fig. 9a), the UF membrane without backwashing exhibited the highest peaks due to the yellow, orange and red colors (Fig. 9b). This phenomenon corresponded to a high "fouling map", as reported in published literature using model foulants (Benavente et al., 2016; Thygesen et al., 2014). In comparison,
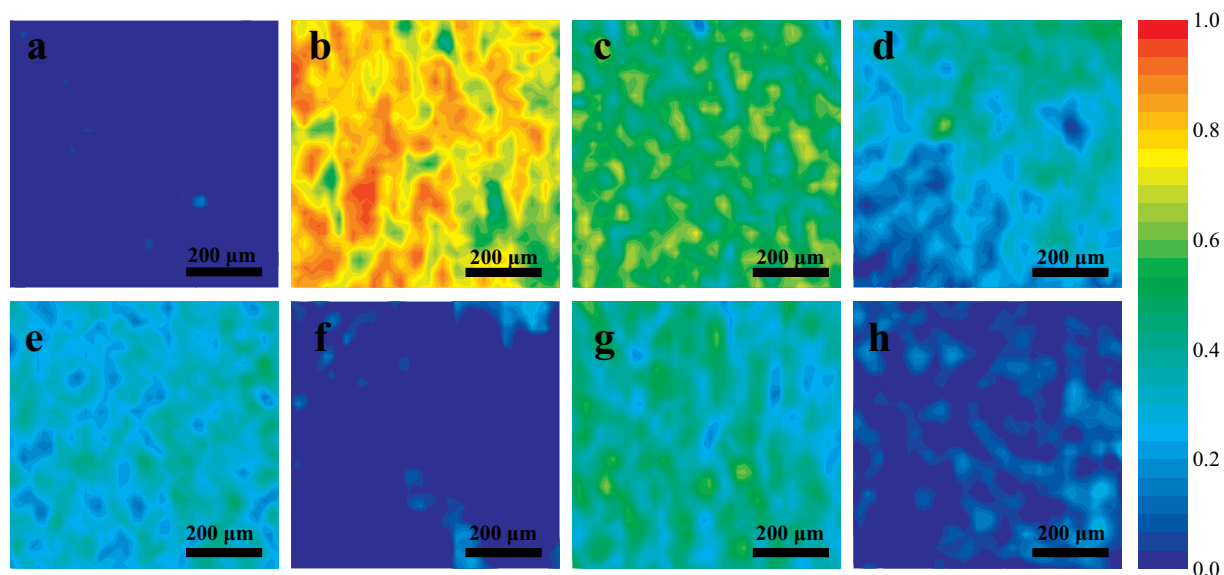
Fig. 9. FTIR microscope maps of (a) virgin membrane, and UF membranes cleaned by various backwash water sources: (b) without backwashing, (c) UF permeate, (d) ultrapure water, (e) NF permeate, (f) RO permeate, (g) RO concentrate and (h) FO draw solution.

the green and yellow colors represented high peaks for the membrane cleaned by UF permeate (Fig. 9c). In addition, the visible images of UF membranes backwashed by UF permeate or without backwashing displayed a dark color (Figs. S9b-c, Supporting Information), probably due to the larger thickness of foulants on the surface. In contrast, the UF membrane backwashed with ultrapure water displayed a lower fouling map due to the low peak intensity of the sample (blue and green), as presented in Fig. 9d. NF permeate and RO concentrate backwashing resulted in higher fouling maps on membrane surfaces than ultrapure water backwashing, but lower than UF permeate backwashing or without backwashing. As expected, a very low fouling intensity was obtained when RO permeate or FO draw solution was used as backwash water (Fig. 9f and h), considering the similar color map with the virgin membrane. The surface mapping technique using FTIR microscopy has been used for qualitative or quantitative analysis of foulants (e.g., proteins) or shales (Benavente et al., 2016; Chen et al., 2014; Miller et al., 2013). Similar to those with a given wavenumber scanning in literature (Benavente et al., 2016; Lien et al., 2018; Xie et al., 2017), the FTIR microscope mapping with full wavenumber scanning showed an overall observation of the UF membrane surface.

3.5. Potential application of backwash water adjustment and implications

Aiming at alleviating UF membrane fouling caused by shale gas FPW, various backwash water sources from UF-NF, UF-RO, UF-NF-RO and UF-FO processes were investigated. Compared to the severe fouling using UF permeate backwashing, the superiority of ultrapure water backwashing was probably due to release of the electric double layer and swelling of fouling layer (Chang et al., 2015; Li et al., 2012; Resosudarmo et al., 2013). The same mechanisms were involved in RO permeate backwashing because the water quality characteristics of RO permeate were similar to ultrapure water (Table 1), and similar UF fouling alleviation was reported for ultrafiltration of seawater (Resosudarmo et al., 2013). Regarding NF permeate, in addition to the swelling of cake layer, the bridging effect of divalent cations may be involved and this was related with decreased cleaning efficiency (Li et al., 2009), while ion exchange of Na^+ with the bound divalent cations (e.g., Ca^{2+} and Ba^{2+}) in the fouling layer improved backwash efficiency. By optimizing hydraulic condition (e.g., pulse backwash), alleviated UF fouling could be obtained using RO concentrate backwashing (Gao et al., 2016; Gilabert-Oriol et al., 2015). Different to UF-RO process, RO concentrate was acquired from NF permeate in the integrated UF-NF-RO process, with primary water parameters two times that of NF permeate, thus, RO concentrate backwashing also involved the same mechanisms for NF permeate backwashing. The swelling of fouling layer and ion exchange of Na^+ with bound divalent cations were primary reasons for the best UF fouling control behavior of the FO draw solution (Fig. 3) which primarily contained NaCl solution (Table 1).

Membrane-based processes are appropriate technologies for treating and recycling shale gas FPW for beneficial reuse (Chang et al., 2019a; Shaffer et al., 2013). The typical integrated processes of these membrane technologies including UF-NF, UF-RO, UF-NF-RO and UF-FO processes using UF membrane as the pretreatment of desalination unit. The process of UF-NF-RO (Alzahrani et al., 2013; Song et al., 2015) was considered to alleviate RO membrane fouling (Fig. S2, Supporting Information). Then, the RO concentrate was an appropriate backwash solution for fouling alleviation of UF membranes in UF-NF-RO process. Besides, the diluted FO draw solution could be used for agricultural irrigation (Kim et al., 2017; Suwaileh et al., 2019), providing widespread application for diluted FO draw solution. Therefore, RO concentrate from the UF-NF-RO process and diluted FO draw solution from the UF-FO process were proposed as appropriate backwash water for UF membrane cleaning.

4. Conclusion

In this study, we used various backwash water sources for cleaning UF fouling caused by shale gas FPW. The following conclusions can be drawn:

1) The fluorescence EEM showed that the organics in shale gas FPW were primarily protein-like substances. The fluorescence intensity in the backwash water decreased with the order: UF permeate > RO concentrate > NF permeate > RO permeate > FO draw solution.
2) Different to severe fouling using UF permeate backwashing, the NF permeate, RO permeate and ultrapure water backwashing led to much lower and comparable FR_t and FR_{nbw} for both hollow fiber and flat-sheet membranes. RO concentrate was an appropriate backwash solution for fouling alleviation of UF membranes in UF-NF-RO process. FO draw solution backwashing resulted in the best membrane control performance, with fouling rates even lower than that in integrated coagulation-UF process under optimal dosage (200 mg/L).
3) The mass of residual foulants on membrane correlated well with non-backwashable fouling parameters including FR_{nbw} and $\triangle R_{nbw}/\triangle R_t$. Significant correlation was observed between the total surface tension of fouled membranes and FR_t.
4) The superiority of ultrapure water, NF permeate, RO permeate, RO concentrate and FO draw solution as backwash water to UF permeate was confirmed by SEM-EDS observation and FTIR spectra. Further, FTIR microscopic mapping technique was a powerful tool for characterizing UF membrane fouling by raw shale gas FPW.

Declaration of Competing Interest

None.

Appendix A. Supplementary data

Supplementary data to this article can be found online at https://doi.org/10.1016/j.envint.2019.05.063.

References

Acharya, H.R., Henderson, C., Matis, H., Kommepalli, H., Moore, B., Wang, H., 2011. Cost Effective Recovery of Low-TDS Frac Flowback Water for Re-use: Final Report. U.S. Department of Energy, Washington, DC.

Alzahrani, S., Mohammad, A.W., Hilal, N., Abdullah, P., Jaafar, O., 2013. Comparative study of NF and RO membranes in the treatment of produced water—part I: assessing water quality. Desalination 315, 18–26.

ASTM International, 2014. Standard Test Method for Silt Density Index (SDI) of Water. (West Conshohocken, PA).

Baker, M.J., Trevisan, J., Bassan, P., Bhargava, R., Butler, H.J., Dorling, K.M., Fielden, P.R., Fogarty, S.W., Fullwood, N.J., Heys, K.A., Hughes, C., Lasch, P., Martin-Hirsch, P.L., Obinaju, B., Sockalingum, G.D., Sulé-Suso, J., Strong, R.J., Walsh, M.J., Wood, B.R., Gardner, P., Martin, F.L., 2014. Using Fourier transform IR spectroscopy to analyze biological materials. Nat. Protoc. 9, 1771–1791.

Barbot, E., Vidic, N.S., Gregory, K.B., Vidic, R.D., 2013. Spatial and temporal correlation of water quality parameters of produced waters from Devonian-age shale following

hydraulic fracturing. Environ. Sci. Technol. 47, 2562–2569.

Bell, E.A., Poynor, T.E., Newhart, K.B., Regnery, J., Coday, B.D., Cath, T.Y., 2017. Produced water treatment using forward osmosis membranes: evaluation of extended-time performance and fouling. J. Membr. Sci. 525, 77–88.

Benavente, L., Coetsier, C., Venault, A., Chang, Y., Causserand, C., Bacchin, P., Aimar, P., 2016. FTIR mapping as a simple and powerful approach to study membrane coating and fouling. J. Membr. Sci. 520, 477–489.

Chang, Y., Huang, R., Ries, R.J., Masanet, E., 2014. Shale-to-well energy use and air pollutant emissions of shale gas production in China. Appl. Energy 125, 147–157.

Chang, H., Qu, F., Liu, B., Yu, H., Li, K., Shao, S., Li, G., Liang, H., 2015. Hydraulic irreversibility of ultrafiltration membrane fouling by humic acid: effects of membrane properties and backwash water composition. J. Membr. Sci. 493, 723–733.

Chang, H., Liang, H., Qu, F., Ma, J., Ren, N., Li, G., 2016a. Towards a better hydraulic cleaning strategy for ultrafiltration membrane fouling by humic acid: effect of backwash water composition. J. Environ. Sci. 43, 177–186.

Chang, H., Liang, H., Qu, F., Shao, S., Yu, H., Liu, B., Gao, W., Li, G., 2016b. Role of backwash water composition in alleviating ultrafiltration membrane fouling by sodium alginate and the effectiveness of salt backwashing. J. Membr. Sci. 499, 429–441.

Chang, H., Liang, H., Qu, F., Liu, B., Yu, H., Du, X., Li, G., Snyder, S.A., 2017. Hydraulic backwashing for low-pressure membranes in drinking water treatment: a review. J. Membr. Sci. 540, 362–380.

Chang, H., Li, T., Liu, B., Vidic, R.D., Elimelech, M., Crittenden, J.C., 2019a. Potential and implemented membrane-based technologies for the treatment and reuse of flowback and produced water from shale gas and oil plays: a review. Desalination 455, 34–57.

Chang, H., Liu, B., Yang, B., Yang, X., Guo, C., He, Q., Liang, S., Chen, S., Yang, P., 2019b. An integrated coagulation-ultrafiltration-nanofiltration process for internal reuse of shale gas flowback and produced water. Sep. Purif. Technol. 211, 310–321.

Chen, W., Westerhoff, P., Leenheer, J.A., Booksh, K., 2003. Fluorescence excitation - emission matrix regional integration to quantify spectra for dissolved organic matter. Environ. Sci. Technol. 37, 5701–5710.

Chen, B.-K., Su, C.-T., Tseng, M.-C., Tsay, S.-Y., 2006. Preparation of polyetherimide nanocomposites with improved thermal, mechanical and dielectric properties. Polym. Bull. 57, 671–681.

Chen, Y., Furmann, A., Mastalerz, M., Schimmelmann, A., 2014. Quantitative analysis of shales by KBr-FTIR and micro-FTIR. Fuel 116, 538–549.

Chen, G., Wang, Z., Nghiem, L.D., Li, X.-M., Xie, M., Zhao, B., Zhang, M., Song, J., He, T., 2015. Treatment of shale gas drilling flowback fluids (SGDFs) by forward osmosis: membrane fouling and mitigation. Desalination 366, 113–120.

Corbatón-Báguena, M.-J., Álvarez-Blanco, S., Vincent-Vela, M.-C., 2014. Cleaning of ultrafiltration membranes fouled with BSA by means of saline solutions. Sep. Purif. Technol. 125, 1–10.

Du, X., Zhang, Z., Carlson, K.H., Lee, J., Tong, T., 2018. Membrane fouling and reusability in membrane distillation of shale oil and gas produced water: effects of membrane surface wettability. J. Membr. Sci. 567, 199–208.

Estrada, J.M., Bhamidimarri, R., 2016. A review of the issues and treatment options for wastewater from shale gas extraction by hydraulic fracturing. Fuel 182, 292–303.

Fakhru'l-Razi, A., Pendashteh, A., Abdullah, L.C., Biak, D.R.A., Madaeni, S.S., Abidin, Z.Z., 2009. Review of technologies for oil and gas produced water treatment. J. Hazard. Mater. 170, 530–551.

Gao, L.X., Rahardianto, A., Gu, H., Christofides, P.D., Cohen, Y., 2016. Novel design and operational control of integrated ultrafiltration — reverse osmosis system with RO concentrate backwash. Desalination 382, 43–52.

Gilabert-Oriol, G., Hassan, M., Dewisme, J., Garcia-Molina, V., Busch, M., 2015. Backwashing pressurized ultrafiltration using reverse osmosis brine in seawater desalination and its potential costs savings. Desalination Water Treat 55, 2800–2812.

Gorzalski, A.S., Donley, C., Coronell, O., 2017. Elemental composition of membrane foulant layers using EDS, XPS, and RBS. J. Membr. Sci. 522, 31–44.

Guo, C., Chang, H., Liu, B., He, Q., Xiong, B., Kumar, M., Zydney, A.L., 2018. An ultrafiltration- reverse osmosis combined process for external reuse of Weiyuan shale gas flowback and produced water. Environ. Sci.: Water Res. Technol. 4, 942–955.

He, C., Wang, X., Liu, W., Barbot, E., Vidic, R.D., 2014. Microfiltration in recycling of Marcellus shale flowback water: solids removal and potential fouling of polymeric microfiltration membranes. J. Membr. Sci. 462, 88–95.

He, M., Chen, W.J., Tian, L., Shao, B., Lin, Y., 2019. Plant-microbial synergism: an effective approach for the remediation of shale-gas fracturing flowback and produced water. J. Hazard. Mater. 363, 170–178.

IEA, 2012. Golden Rules for a Golden Age of Gas: World Energy Outlook – Special Report on Unconventional Gas. World Energy Outlook 2012, International Energy Agency, Paris, France.

Jiang, Q., Rentschler, J., Perrone, R., Liu, K., 2013. Application of ceramic membrane and ion-exchange for the treatment of the flowback water from Marcellus shale gas production. J. Membr. Sci. 431, 55–61.

Jiang, S., Li, Y., Ladewig, B.P., 2017. A review of reverse osmosis membrane fouling and control strategies. Sci. Total Environ. 595, 567–583.

Kim, Y., Li, S., Chekli, L., Phuntsho, S., Ghaffour, N., Leiknes, T., Shon, H.K., 2017. Influence of fertilizer draw solution properties on the process performance and microbial community structure in a side-stream anaerobic fertilizer-drawn forward osmosis - ultrafiltration bioreactor. Bioresour. Technol. 240, 149–156.

Kondash, A., Vengosh, A., 2015. Water footprint of hydraulic fracturing. Environ. Sci. Technol. Lett. 2, 276–280.

Kong, F.-X., Sun, G.-D., Chen, J.-F., Han, J.-D., Guo, C.-M., Tong-Zhang, Lin, X.-F., Xie, Y.F., 2018. Desalination and fouling of NF/low pressure RO membrane for shale gas

fracturing flowback water treatment. Sep. Purif. Technol. 195, 216–223.

Li, S., Heijman, S.G.J., Verberk, J.Q.J.C., Verliefde, A.R.D., Kemperman, A.J.B., van Dijk, J.C., Amy, G., 2009. Impact of backwash water composition on ultrafiltration fouling control. J. Membr. Sci. 344, 17–25.

Li, S., Heijman, S.G.J., Verberk, J.Q.J.C., Verliefde, A.R.D., Amy, G.L., van Dijk, J.C., 2012. Removal of different fractions of NOM foulants during demineralized water backwashing. Sep. Purif. Technol. 98, 186–192.

Li, X.-M., Zhao, B., Wang, Z., Xie, M., Song, J., Nghiem, L.D., He, T., Yang, C., Li, C., Chen, G., 2014. Water reclamation from shale gas drilling flow-back fluid using a novel forward osmosis-vacuum membrane distillation hybrid system. Water Sci. Technol. 69, 1036–1044.

Lien, C.-C., Yeh, L.-C., Venault, A., Tsai, S.-C., Hsu, C.-H., Dizon, G.V., Huang, Y.-T., Higuchi, A., Chang, Y., 2018. Controlling the zwitterionization degree of alternate copolymers for minimizing biofouling on PVDF membranes. J. Membr. Sci. 565, 119–130.

Liu, F., Hashim, N.A., Liu, Y., Abed, M.R.M., Li, K., 2011. Progress in the production and modification of PVDF membranes. J. Membr. Sci. 375, 1–27.

Maltos, R.A., Regnery, J., Almaraz, N., Fox, S., Schutter, M., Cath, T.J., Veres, M., Coday, B.D., Cath, T.Y., 2018. Produced water impact on membrane integrity during extended pilot testing of forward osmosis – reverse osmosis treatment. Desalination 440, 99–110.

Miller, L.M., Bourassa, M.W., Smith, R.J., 2013. FTIR spectroscopic imaging of protein aggregation in living cells. Biochim. Biophys. Acta 1828, 2339–2346.

Murphy, K.R., Butler, K.D., Spencer, R.G., Stedmon, C.A., Boehme, J.R., Aiken, G.R., 2010. Measurement of dissolved organic matter fluorescence in aquatic environments: an interlaboratory comparison. Environ. Sci. Technol. 44, 9405–9412.

Rabuni, M.F., Nik Sulaiman, N.M., Aroua, M.K., Hashim, N.A., 2013. Effects of alkaline environments at mild conditions on the stability of PVDF membrane: an experimental study. Ind. Eng. Chem. Res. 52, 15874–15882.

Reig, P., Luo, T., Proctor, J.N., 2014. Global Shale Gas Development: Water Availability and Business Risks. World Resources Institute.

Resosudarmo, A., Ye, Y., Le-Clech, P., Chen, V., 2013. Analysis of UF membrane fouling mechanisms caused by organic interactions in seawater. Water Res. 47, 911–921.

Riley, S.M., Oliveira, J.M.S., Regnery, J., Cath, T.Y., 2016. Hybrid membrane bio-systems for sustainable treatment of oil and gas produced water and fracturing flowback water. Sep. Purif. Technol. 171, 297–311.

Riley, S.M., Ahoor, D.C., Regnery, J., Cath, T.Y., 2018. Tracking oil and gas wastewater-derived organic matter in a hybrid biofilter membrane treatment system: a multi-analytical approach. Sci. Total Environ. 613-614, 208–217.

Roy, S., Thakur, P., Hoque, N.A., Bagchi, B., Sepay, N., Khatun, F., Kool, A., Das, S., 2017. Electroactive and high dielectric folic acid/PVDF composite film rooted simplistic organic photovoltaic self-charging energy storage cell with superior energy density and storage capability. ACS Appl. Mater. Interfaces 9, 24198–24209.

Sari, M.A., Chellam, S., 2015. Mechanisms of boron removal from hydraulic fracturing wastewater by aluminum electrocoagulation. J. Colloid Interface Sci. 458, 103–111.

Shaffer, D.L., Chavez, L.H.A., Ben-Sasson, M., Castrillón, S.R.-V., Yip, N.Y., Elimelech, M., 2013. Desalination and reuse of high-salinity shale gas produced water: drivers, technologies, and future directions. Environ. Sci. Technol. 47, 9569–9583.

Song, Y., Gao, X., Li, T., Gao, C., Zhou, J., 2015. Improvement of overall water recovery by increasing RNF with recirculation in a NF–RO integrated membrane process for seawater desalination. Desalination 361, 95–104.

Subhi, N., Verliefde, A.R.D., Chen, V., Le-Clech, P., 2012. Assessment of physicochemical interactions in hollow fibre ultrafiltration membrane by contact angle analysis. J. Membr. Sci. 403-404, 32–40.

Suhartono, J., Tizaoui, C., 2015. Polyvinylidene fluoride membranes impregnated at optimised content of pristine and functionalised multi-walled carbon nanotubes for improved water permeation, solute rejection and mechanical properties. Sep. Purif. Technol. 154, 290–300.

Sun, M., Zucker, I., Davenport, D.M., Zhou, X., Qu, J., Elimelech, M., 2018. Reactive, self-cleaning ultrafiltration membrane functionalized with iron oxychloride nanocatalysts. Environ. Sci. Technol. 52, 8674–8683.

Suwaileh, W., Johnson, D., Hilal, N., 2019. Brackish water desalination for agriculture: assessing the performance of inorganic fertilizer draw solutions. Desalination 456, 53–63.

Tang, C., Kwon, Y., Leckie, J., 2007. Probing the nano- and micro-scales of reverse osmosis membranes—a comprehensive characterization of physiochemical properties of uncoated and coated membranes by XPS, TEM, ATR-FTIR, and streaming potential measurements. J. Membr. Sci. 287, 146–156.

Tang, C.Y., Kwon, Y.-N., Leckie, J.O., 2009. Effect of membrane chemistry and coating layer on physiochemical properties of thin film composite polyamide RO and NF membranes: I. FTIR and XPS characterization of polyamide and coating layer chemistry. Desalination 242, 149–167.

Thygesen, O., Hedegaard, M.A.B., Zarebska, A., Beleites, C., Krafft, C., 2014. Membrane fouling from ammonia recovery analyzed by ATR-FTIR imaging. Vib. Spectrosc. 72, 119–123.

US EIA, 2013. Technically Recoverable Shale Oil and Shale Gas Resources: An Assessment of 137 Shale Formations in 41 Countries outside the United States. U.S. Department of Energy, Washington, DC.

US EPA, 2005. Membrane filtration guidance manual. United States Environmental Protection Agency, Office of Water.

Voutchkov, N., 2010. Considerations for selection of seawater filtration pretreatment system. Desalination 261, 354–364.

Wan, C., Bowen, C.R., 2017. Multiscale-structuring of polyvinylidene fluoride for energy

harvesting: the impact of molecular-, micro- and macro-structure. J. Mater. Chem. A 5, 3091–3128.

Xie, M., Luo, W., Gray, S.R., 2017. Synchrotron Fourier transform infrared mapping: a novel approach for membrane fouling characterization. Water Res. 111, 375–381.

Xiong, B., Zydney, A.L., Kumar, M., 2016. Fouling of microfiltration membranes by flowback and produced waters from the Marcellus shale gas play. Water Res. 99, 162–170.

Yang, Q., Gao, A., Xue, L., 2017. "Butterfly effect" from finite dope chemical composition variations on the water/oil separation capabilities of super rough polyvinylidene difluoride (PVDF) porous membranes. J. Membr. Sci. 524, 197–204.

Zhang, F., Zhang, W., Yu, Y., Deng, B., Li, J., Jin, J., 2013. Sol–gel preparation of PAA-g-

PVDF/TiO$_2$ nanocomposite hollow fiber membranes with extremely high water flux and improved antifouling property. J. Membr. Sci. 432, 25–32.

Zhang, S., Cao, J., Ma, N., You, M., Wang, X., Meng, J., 2018. Fast and facile fabrication of antifouling and hemocompatible PVDF membrane tethered with amino-acid modified PEG film. Appl. Surf. Sci. 428, 41–53.

Zou, C., Ni, Y., Li, J., Kondash, A., Coyte, R., Lauer, N., Cui, H., Liao, F., Vengosh, A., 2018. The water footprint of hydraulic fracturing in Sichuan Basin, China. Sci. Total Environ. 630, 349–356.

Zularisam, A.W., Ismail, A.F., Salim, R., 2006. Behaviours of natural organic matter in membrane filtration for surface water treatment — a review. Desalination 194, 211–231.